Deformation of Small Compressed Droplets

Martin-D. Lacasse[1], Gary S. Grest[1], and Dov Levine[2]
[1] *Corporate Research Science Laboratories*
Exxon Research and Engineering Co., Annandale, NJ 08801
[2] *Department of Physics, Technion, Haifa, 32000 Israel*
(March 11, 1996)

We investigate the elastic properties of small droplets under compression. The compression of a bubble by two parallel plates is solved exactly and it is shown that a lowest-order expansion of the solution reduces to a form similar to that obtained by Morse and Witten. Other systems are studied numerically and results for configurations involving between 2 and 20 compressing planes are presented. It is found that the response to compression depends on the number of planes. The shear modulus is also calculated for common lattices and the stability crossover between f.c.c. and b.c.c. is discussed.

PACS numbers: 82.70.Kj, 81.40.Jj, 62.20.Dc

I. INTRODUCTION

Emulsions consist of a mixture of two immiscible fluids, one of which, generally an oil, is dispersed as small droplets in the continuous phase of the other fluid, generally water. The interfaces are stabilized by a surfactant, preventing coalescence. Emulsions are materials with quite unusual properties: despite being comprised solely of fluids, they become elastic solids when the droplets are compressed to a large enough volume fraction φ by extracting the continuous phase by the application of an osmotic pressure Π. The origin of the elasticity is the interfacial energy of the droplets. At low volume fractions, the surface tension σ ensures that the droplets are spherical in shape. However, at higher φ, the packing constraints force the droplets to deform, thus storing energy. Consequently, it is a fundamental issue to determine the increase of the surface area of a droplet resulting from an arbitrary deformation.

It is generally believed that the application of a shear strain to a compressed emulsion causes the droplets to further deform, thereby storing more energy [1,2,3,4,5]. According to this picture, the scale of both the osmotic pressure, and the elastic shear modulus G is set by the Laplace pressure of the droplets, $(2\sigma/R)$, where R is the radius of an undeformed droplet. Recent experiments [6] on the elastic properties of compressed monodisperse emulsions of silicone-oil in water confirm the role of the Laplace pressure: the experimental values of G and Π for different droplet sizes, when scaled by (σ/R), collapse on a single curve [6].

Compression modifies the elastic properties of a disordered emulsion, changing the response from liquid-like to solid-like. The onset of solid-like behavior is gradual; both Π and G increase smoothly from zero as the system is compressed above $\varphi_c \approx 0.64$ [6], the volume fraction at which disordered monodisperse droplets are first deformed [7]. For polydisperse emulsions, φ_c is larger [8], reflecting more efficient packing. Two separate elastic responses of the droplets are therefore of interest: to direct compression and to shear.

The increase of the surface area of a droplet under compression comes from the relatively low cost of deformation compared to the compressibility of the internal fluid. Thus, it is very reasonable to assume that the droplets are composed of an incompressible fluid, and may be consequently considered to have a fixed volume. The effect of gravity may be nullified by density matching of the oil and water, but in any case would be tiny because of the large surface tension and small droplet size (typically of a μm) of the experimental systems.

When the droplets are compressed just beyond the point they start to deform, i.e. $\varphi \gtrsim \varphi_c$, they form small facets separated by thin surfactant-water-surfactant films. Each of the facets created on the droplet surface has the effect of *locally* decreasing the droplet surface, but volume conservation makes the droplet *globally* increase its surface, and thus its energy. Due to such nonlocal effects, the determination of the droplet response to compression requires that it be considered as a whole. Consequently, a complete analytic solution is limited to a few simple cases, one of which is a drop squeezed between two parallel plates, to be presented in Section III. The response to shear is still more difficult, but fortunately, numerical tools capable of handling such problems have recently become available [9].

Upon more compression, droplets gradually take the shape of a rounded polyhedron. At this point, the water is contained within the connected network of voids left between the oil droplets. This network is made of thin veins, along which the facets meet, and which connect larger regions located at the corners of the polyhedra. As $\varphi \to 1$, i.e. in the so-called dry foam limit, mechanical equilibrium imposes constraints on these regions which were first discussed by Plateau [10]. In particular, exactly three films meet at equal angles (120°) along the veins which become the edges of the polyhedra. Additionally, the corner regions reduce to a point at which four edges meet at equal tetrahedral angles. These rules do not apply until most of the continuous phase has been extracted.

The elasticity of emulsions has been the object of nu-

merous investigations over the last decade. The first theoretical attempts [1,2] were for ordered lattices in two dimensions, which we shall briefly treat in Section II, mainly in order to contrast them with three-dimensional systems. It should be noted that two-dimensional systems are important in their own right, both theoretically and experimentally. For example, the effects of polydispersity and disorder are largely studied in two dimensions [3,11,12].

For real (three-dimensional) bubbles, the only analytical expression [4] for the behavior of a droplet surface under compression involves the application of an infinitesimal force at a single point. A simplified approach consists in assuming that each droplet becomes a truncated sphere under compression [13]. Using each of these approaches, the shear modulus of a simple cubic (s.c.) lattice has been derived [5]. These studies predict that the onset of the shear modulus at φ_c is discontinuous, in contrast with the smooth quasi-linear increase of G at φ_c found experimentally for disordered emulsions.

The relative importance of the disorder of the emulsions, its polydispersity, and the response of the droplets themselves is the object of current research [14]. This paper is concerned with the last: we present the results of an investigation of the response of an individual droplet to deformation. In Section II we present results for the 2-dimensional case. Section III derives exact results for the compression of a droplet by two parallel plates. In the limit of infinitesimal compression, our results are compared with Morse and Witten's expression [4]. For a large range of compressions, we show that the energy has an anharmonic power-law response to compression. In Section IV, we present numerical results for the compression of a droplet in several local environments using Brakke's Surface Evolver (SE) software [9]. We again demonstrate that the energy of the squeezed droplet is anharmonic, *with the power depending on the number of facets.* Section V describes the results obtained for a selection of space-filling structures at the dry foam limit. Section VI contains numerical calculations of the droplet response to a shear deformation. We discuss our results and conclude in Section VII.

II. RESPONSE IN TWO DIMENSIONS

Two-dimensional systems have characteristics not found in three-dimensions. For example, monodisperse arrays of disks order easily [15] in an hexagonal array of surface fraction $\varphi_c = \pi/(2\sqrt{3}) \approx 0.9069$. The elastic properties of two-dimensional ordered systems have been discussed extensively by Princen [1,16]. The response to deformation is also simpler in two dimensions. A minimum free surface (a free curve in the present case) is characterized by a uniform pressure or, equivalently by a constant mean curvature. In two dimensions, the surface is parameterized by only one radius of curvature and the minimum free surface is therefore always an arc of a circle.

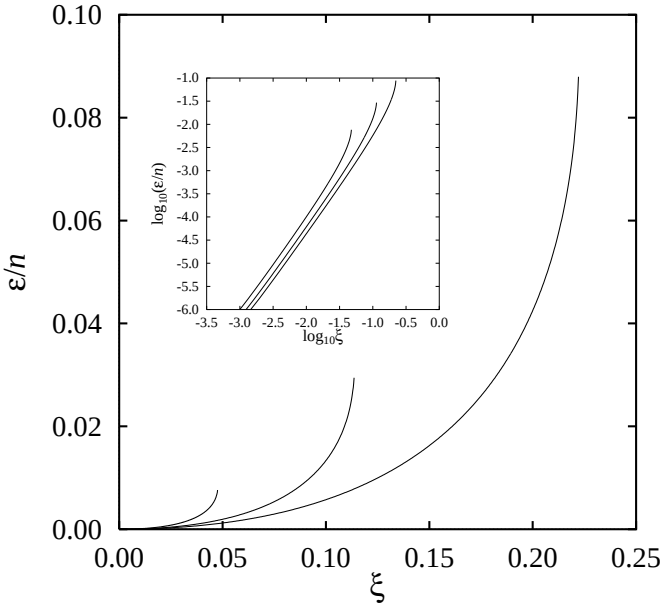

FIG. 1. The excess energy per facet of a two-dimensional droplet as a function of compression. The curves represent, from right to left, the tessellating cases $n = 3$, 4, and 6. The insert shows the same data on a logarithmic scale.

Let us consider the deformation of a two-dimensional droplet of constant area confined inside a regular polygon of n sides. Only for $n = 3$,4, and 6 can such polygons be tessellated, but we shall consider general n, in particular to contrast the two- and three-dimensional results. The ratio of droplet area to polygon area is denoted by φ. Only for the tessellating cases will φ represent the surface covering fraction of the corresponding lattice. In the following, we assume that the droplet is non-wetting so that the contact angles are zero. At $\varphi_c = \frac{\pi}{n} \cot \frac{\pi}{n}$, the circular droplet is undeformed and touches the polygon at exactly n points, being the midpoints of the polygon's edges. If the polygon is now shrunk uniformly, the droplet will distort, and its new minimum-perimeter shape will consist of small facets joined by circular arcs. As φ increases above φ_c, the length of the flat portions increases and the radius of curvature of the arcs decreases, reflecting increased droplet pressure. At $\varphi = 1$, the radius of curvature of the arcs becomes zero (infinite pressure), and the bubble takes on the shape of the polygonal cell.

The interfacial energy of the droplets is the product of their line tension σ and the perimeter length ℓ. It is convenient to measure the excess energy by the following dimensionless quantity

$$\varepsilon \equiv \frac{\ell}{2\pi R} - 1, \tag{1}$$

where R is the radius of the undeformed circular droplet. Similarly, the degree of compression will be measured by the following dimensionless displacement

$$\xi \equiv \frac{R-h}{R}, \tag{2}$$

where h is the perpendicular distance from the facets to the center of the droplet. ξ is simply related to the volume fraction through $\xi = 1 - \sqrt{\varphi_c/\varphi}$. For any regular polygonal cell, ε can be shown to be, for $\varphi \geq \varphi_c$,

$$\varepsilon = \frac{1}{\sqrt{\varphi\varphi_c}} - \sqrt{\frac{(1-\varphi)(1-\varphi_c)}{\varphi\varphi_c}} - 1. \tag{3}$$

For φ slightly greater than φ_c, we may expand the previous expression in terms of $(\varphi - \varphi_c)$, and get

$$\begin{aligned} \varepsilon &\approx \left(\frac{1}{8\varphi_c^2(1-\varphi_c)}\right)(\varphi-\varphi_c)^2, \\ &\approx \left(\frac{1}{2(1-\varphi_c)}\right)\xi^2. \end{aligned} \tag{4}$$

Therefore, for small compression, the energy is harmonic, and the prefactor depends on the number of faces of the polygon through φ_c. This is shown in Fig. 1 where the excess energy per facet is plotted for the tessellating cases $n = 3$, 4 and 6. The end of each curve corresponds to $\varphi \to 1$ for each lattice. The logarithmic insert shows the wide range over which harmonicity holds as well as the n dependence of the prefactor expressed by the different intercepts.

In two dimensions, the scaled osmotic pressure can be obtained from

$$\Pi/(\sigma/R) = 2\varphi^2 \frac{\partial \varepsilon}{\partial \varphi}, \tag{5}$$

and we find, using Eq. 3,

$$\Pi/(\sigma/R) = \left(\frac{\varphi}{\varphi_c}\right)^{\frac{1}{2}} \left[\left(\frac{1-\varphi_c}{1-\varphi}\right)^{\frac{1}{2}} - 1\right]. \tag{6}$$

This last expression, which depends on n through φ_c, is valid for all tessellations in two dimensions. For $\varphi \gtrsim \varphi_c$, Π can be shown to increase linearly with $(\varphi - \varphi_c)$.

In the model proposed by Princen [1,16], droplets are monodisperse cylindrical objects packed in an hexagonal array ($n = 6$). In the dry foam limit, this configuration satisfies Plateau's rules for packing in two dimensions. For $\varphi > \varphi_c$, the osmotic pressure is given by Eq. 6, with $n = 6$ [11,16]. For the same range, the static shear modulus was found to obey [1]

$$G/(\sigma/R) = 0.525\varphi^{\frac{1}{2}}. \tag{7}$$

Thus, this model predicts a discontinuity of G at φ_c, its value jumping from zero to $0.525\sqrt{\varphi_c}$. The onset of the shear modulus is thus very sharp at φ_c, and we shall demonstrate that this elastic response is intimately associated with the response of the droplet potential at $\xi \to 0$.

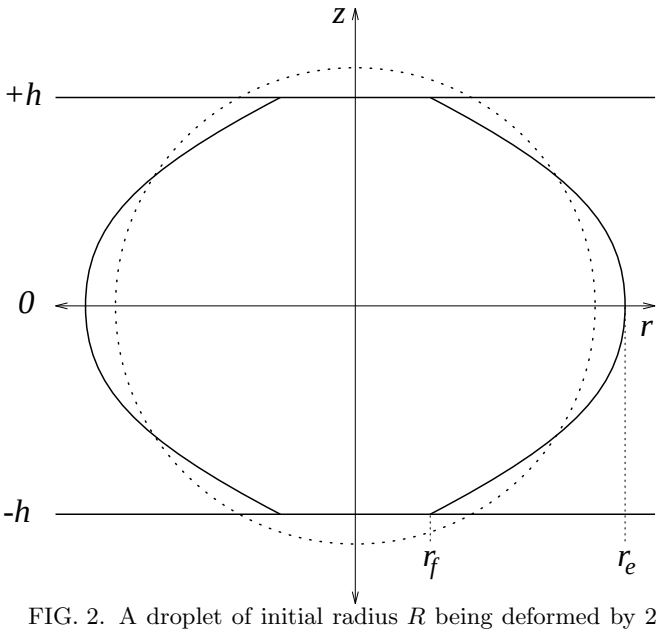

FIG. 2. A droplet of initial radius R being deformed by 2 parallel plates located at $z = -h$ and $z = +h$. The equator is located at $z = 0$ and has a radius r_e. Both facets at $z = \pm h$ are circular and have a radius r_f. The droplet shape is a cubic spline drawn for visualization purposes only.

III. COMPRESSION BY TWO PLATES

The evaluation of the excess energy stored in an arbitrary surface deformation of a compressed droplet is a difficult problem. A simple three-dimensional case consists of a droplet of radius R compressed between two parallel planes, each located at a distance h from the center of the droplet (*cf.* Fig. 2). We shall measure compression by the dimensionless ratio ξ defined as above. At small compression $d\xi$, small circular facets of radius r_f appear where the droplet touches each plate. Naively, the resulting force dF on each facet can be estimated by assuming that the radius of the droplet, and hence the Laplace pressure, remains unchanged. Therefore, $dF \approx (2\sigma/R)dS$, where dS is the surface of the flattened facet. To lowest order in the deformation,

$$dS \approx 2\pi R^2 d\xi, \tag{8}$$

so that $dF \approx 4\pi\sigma R d\xi$. Thus, to lowest order, the response of a droplet compressed between 2 parallel plates is found to be identical to the compression of a repulsive harmonic spring of spring constant $4\pi\sigma$. However, this simple derivation leads to a wrong answer, as we now show.

Because of its azimuthal symmetry, we may express this problem as a one-dimensional problem, that of finding the solid of revolution of a constant volume with minimum surface area. The free surface of this solid is given by a curve $r(z)$ rotated about the z-axis. The mathematical aspects of the present problem, such as stability

and the existence of a solution as a function of contact angles, have recently been discussed in detail by various authors [17,18,19,20].

Using the Euler-Lagrange formalism, we minimize the total droplet surface, A, which is given by

$$A = 2\pi r_f^2 + 2\int_{-h}^{0} 2\pi r\sqrt{1+r_z^2}\, dz \tag{9}$$

where $r_z \equiv dr/dz$. The minimization is done under the constraint of constant volume:

$$\frac{4}{3}\pi R^3 = 2\int_{-h}^{0} \pi r^2\, dz, \tag{10}$$

which is introduced through the use of a Lagrange multiplier λ in a function $\mathcal{L}$,

$$\mathcal{L} = \frac{r_f^2}{h} + 2r\sqrt{1+r_z^2} - \lambda r^2 \tag{11}$$

to be minimized. Since $\mathcal{L} = \mathcal{L}(r, r_z)$ is independent of z, one can use the integrated form of the Euler-Lagrange equation [21]

$$r_z \frac{\partial \mathcal{L}}{\partial r_z} - \mathcal{L} = C, \tag{12}$$

where C is an integration constant. We re-express the unknown constants λ and C using the following boundary conditions:

$$r_z|_{r_f} = \infty, \tag{13a}$$
$$r_z|_{r_e} = 0, \tag{13b}$$

where r_e is the maximum value of r located at the equator (*cf.* Fig. 2). The first condition sets the contact angle at the facet, which should be zero if no long-range attractive forces are present [1,13]. The second comes from symmetry and macroscopic smoothness at the equator.

It will be convenient to use the following dimensionless variables

$$\rho = r/r_e, \tag{14a}$$
$$\rho_f = r_f/r_e, \tag{14b}$$
$$\zeta = z/r_e, \tag{14c}$$

and, including these changes, Eq. 12 reads

$$\sqrt{1+\rho_\zeta^2} = \frac{\rho(1-\rho_f^2)}{\rho^2-\rho_f^2}. \tag{15}$$

Solving for z and integrating, we get

$$z = -h + r_e I(\rho), \tag{16}$$

where ρ goes from ρ_f to 1, and $I(\rho)$ is an integral that can be solved at least numerically, and which is given by

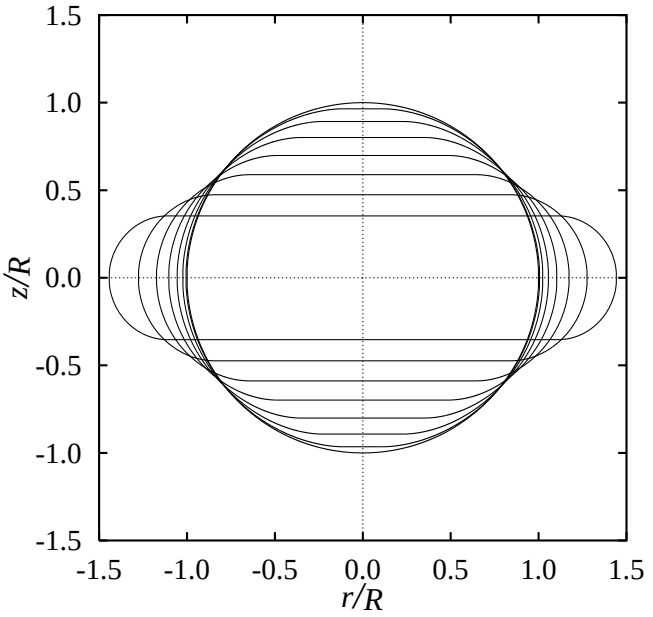

FIG. 3. Shape of a droplet compressed between two parallel plates for different plate displacements: $\xi = 0.000$, 0.035, 0.107, 0.199, 0.302, 0.411, 0.526, 0.647.

$$I(\rho) = \int_{\rho_f}^{\rho} \frac{x^2-\rho_f^2}{\sqrt{(1-x^2)(x^2-\rho_f^4)}}\, dx. \tag{17}$$

Setting $z = 0$ in Eq. 16 we obtain a relation between h/r_e and ρ_f:

$$h = r_e I_1 \tag{18}$$

where $I_1 \equiv I(1)$. This allows us to re-express Eq. 16 as

$$z = -h\left[1 - I(\rho)/I_1\right]. \tag{19}$$

We note here that both $I(\rho)$ and I_1 are functions of ρ_f, which in turn is related to h through the volume constraint, Eq. 10. Using Eqs. 10 and 18, h can be related to ρ_f through the following non-trivial relation

$$h = RI_1\left(\frac{2}{3J_1}\right)^{1/3}, \tag{20}$$

where J_1 is another integral defined by

$$J_1 = \int_{\rho_f}^{1} \frac{x^2(x^2-\rho_f^2)}{\sqrt{(1-x^2)(x^2-\rho_f^4)}}\, dx. \tag{21}$$

At this point the problem is fully determined. Given the size of the facets r_f, the plate separation $2h$ is determined by Eq. 20, and the shape of the droplet by Eq. 19. The total droplet surface is obtained by combining Eqs 9, 15, and 18, to get

$$A = \frac{2\pi h^2}{I_1^2}\left[\rho_f^2 + 2(1-\rho_f^2)K_1\right], \tag{22}$$

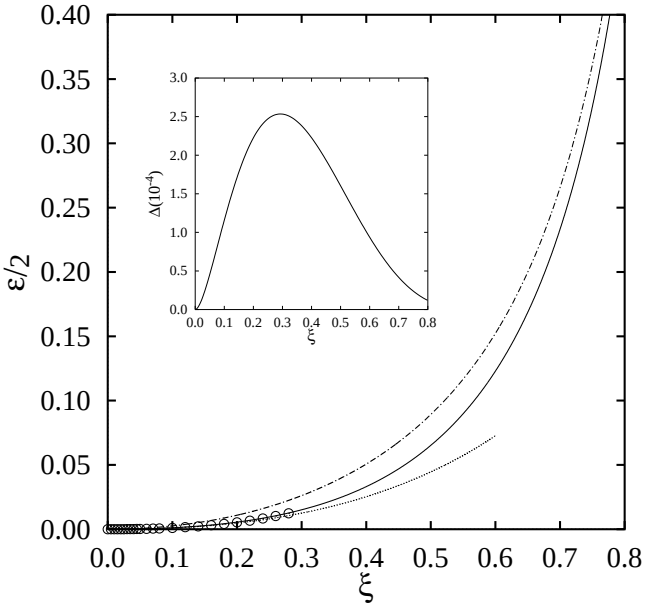

FIG. 4. Relative excess energy per facet for a single droplet as a function of the dimensionless displacement ξ. Curves are, from top to bottom: the truncated sphere approximation (dot-dashed), the exact solution (solid), and the potential predicted by Eq. 32 (dotted). Data points ($\circ$) are results obtained from SE. The absolute difference Δ in ε between the semi-circular surface approximation and the exact solution is shown as an insert.

where K_1 is yet another integral defined by

$$K_1 = \int_{\rho_f}^{1} \frac{x^2}{\sqrt{(1-x^2)(x^2-\rho_f^4)}}\, dx. \tag{23}$$

The integrals I_1, J_1, and K_1 are elliptic integrals which we can solve numerically, after removing the divergence at $x = 1$ by direct analytical integration. The solution of Eq. 19, for various values of h, leads to the different droplet shapes shown in Fig. 3.

It is convenient to define the (dimensionless) relative droplet excess surface energy by

$$\varepsilon \equiv A/(4\pi R^2) - 1. \tag{24}$$

Figure 4 shows the relative excess energy as derived from Eq. 22. It is interesting to compare our solution to different estimates, which model the deformed droplets in different ways. For example, we consider the relative excess energy of a body of equal volume consisting of a cylinder of radius r_f' surrounded by a semi-circle of revolution of radius h. This solution has a zero contact angle for all compressions and becomes exact in the two displacement limits $\xi \to 0$, and $\xi \to 1$. Given the scale of Fig. 4, it is not possible to distinguish the results of this estimate from the exact solution, and we thus show the difference as an insert. A second estimate which has been used in the case of compression by multiple planes [5,13] consists in considering a truncated sphere having the same volume. Results from this estimate are also shown in Fig. 4. The force required to compress the plates is a better accuracy indicator, and forces derived from each solution will be compared below.

The integrals I_1, J_1 and K_1 can be solved analytically when $\rho_f = 0$, i.e., for the undeformed sphere. Let us consider small compressions, and expand the integrals about $\rho_f = 0$. For K_1, for instance, we obtain

$$K_1 \approx \int_{\rho_f}^{1} \left(\frac{x^2}{x\sqrt{1-x^2}} + \frac{\rho_f^4}{2} \frac{x^2}{x^3\sqrt{1-x^2}} \right) dx, \tag{25}$$

which becomes, after performing the integrals,

$$K_1 \approx 1 - \frac{\rho_f^2}{2} + \frac{\rho_f^4}{2}\left[\ln(2) - \frac{1}{4} - \ln(\rho_f) \right]. \tag{26}$$

In this limit one finds, after expanding Eq.22 in a similar way,

$$\varepsilon \approx -4X^2 \left(\ln(X) + \frac{1}{2} \right), \tag{27}$$

where

$$X \equiv (\rho_f/2)^2 \tag{28}$$

has been introduced for simplicity. Using similar expansions in Eq. 20, one obtains

$$\xi \approx -2X \ln(X). \tag{29}$$

Due to this non-trivial relation, we cannot express ε in terms of ξ. It is possible, however, to combine Eqs. 27 and 28 to obtain an expression for the dimensionless force f

$$f \equiv \frac{d\varepsilon}{d\xi} \approx 4X. \tag{30}$$

Combining the last equations, we may re-express the excess energy in terms of f:

$$\varepsilon \approx \frac{1}{4} f^2 \left[k - \ln(f) \right], \tag{31}$$

where the constant $k = 2\ln(2) - \frac{1}{2}$. Morse and Witten [4] obtained a similar result by considering, to lowest-order, a point perturbation of a sphere. In order to test the range of validity of our expansion, we solve Eq. 31 numerically to obtain $\varepsilon(\xi)$. This is done by transforming Eq. 31 into a self-consistent integral equation

$$f(\xi) = \left(\frac{4\int_0^{\xi} f(x)dx}{k - \ln(f(\xi))} \right)^{1/2}, \tag{32}$$

from which $\varepsilon(\xi) = \int_0^{\xi} f(x)dx$ is obtained after a few tens of iterations only. The results are shown by the dotted lines on Figures 4 and 5.

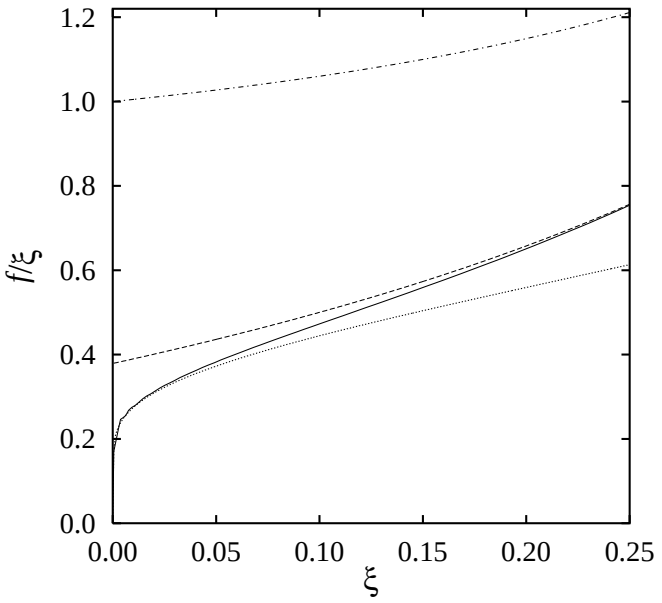

FIG. 5. A comparison of the ξ dependence of the dimensionless force ratio f/ξ for different solutions. Curves are, top to bottom: the truncated sphere approximation (dot-dashed), the semi-circular surface approximation (dashed), the exact solution (solid), and its lowest-order expansion (dotted).

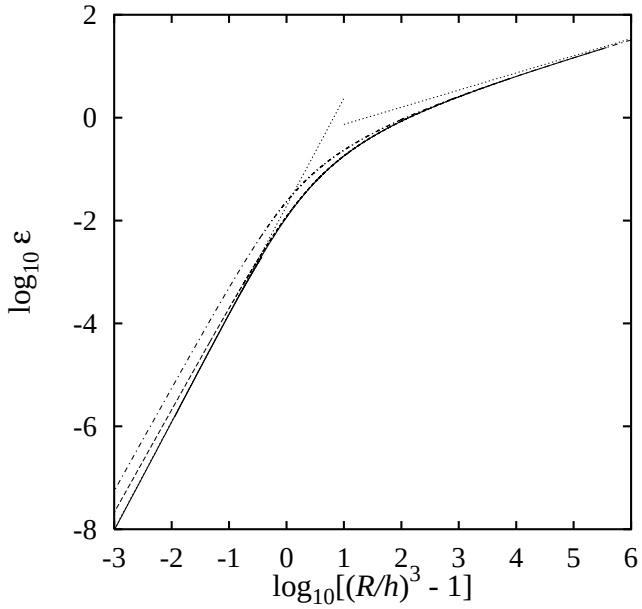

FIG. 6. Logarithmic plot of the relative excess energy versus the displacement function $[(R/h)^3 - 1]$. A simple power law describes the data very well at low compression, as shown by the dotted line. The low-compression fits a slope of 2.1 while the high-compression data joins the asymptotic limit of slope $\frac{1}{3}$. Curves are, top to bottom: truncated sphere approximation (dot-dashed), semi-circular surface approximation (dashed), and exact (solid).

Thus, we showed that the response of a droplet to compression is not harmonic, even to lowest order. It is not possible to obtain an expression for the potential as a function of ξ in closed form, given the presence of elliptic integrals. It is possible, however, to test phenomenological expressions from our exact results. For this purpose, the divergence of the excess energy at $h \to 0$ is not of particular interest given the perspective of a droplet packing. We shall therefore concentrate on the droplet response to small compression.

It is instructive to compare the forces predicted by the different estimates to the exact results. Figure 5 shows the ratio f/ξ for the exact solution, its lowest-order expansion (Eq. 31), the semi-circular surface model, and the truncated sphere model. A harmonic potential would be represented by a constant value in such a plot. For $\xi \lesssim 0.001$, the exact solution sharply drops to zero as does its lowest order expansion. On the other hand, as ξ goes to zero, the semi-circular surface model goes to $(2 - 16/\pi^2)$, showing that the potential becomes harmonic as $\xi \to 0$. Finally, the truncated sphere model is found to be closer to a harmonic potential, having a smaller relative variation in f/ξ. There are two essential characteristics of the exact force. The first one is the anharmonic behavior of the force at $\xi \to 0$. This feature is responsible for the logarithmic onset of G at φ_c predicted for ordered emulsions [5]. The second essential characteristic is that f/ξ increases as the displacement increases. These important features, we believe, are responsible for the characteristic positive curvature of G observed for disordered droplet packings.

An approximate functional form for the droplet potential would be useful in providing estimates of the elastic properties of compressed emulsions. For this purpose, the increase of f/ξ with the displacement can either be approximated by a power law ξ^α with $\alpha > 2$ or by the addition of higher-order terms to a harmonic potential. The former is preferred however, both for its simplicity and because it vanishes as $\xi \to 0$, similar to the exact solution.

In view of investigating fitting functions, a logarithmic plot of ε in terms of $[(R/h)^3 - 1]$ is presented in Fig. 6. The numerical solution of Eq. 31 can be performed with a precision larger than the one optimally possible when solving directly for ε (Eq. 22). Therefore, the low-compression values of ε shown on Fig. 6 were obtained using the lowest-order expansion (Eq. 32). There are two distinct behaviors separated by a crossover section. By approximating the droplet by a compressed cylinder, it can easily be shown that $\varepsilon \sim 1/h$ as $h \to 0$. This asymptotic limit is represented by the dotted line of slope 1/3 at high abscissa values. At low compression, the data are relatively well described by a power law of the form ξ^α or $[(\frac{R}{h})^3 - 1]^\alpha$. We found that the latter provides a better fit over a wider range of h. It also has the advantage of simplifying to the form $(\varphi - \varphi_c)^\alpha$ for space-filling polyhedra. Moreover, the two forms are equivalent for small ξ since $[(\frac{R}{h})^3 - 1] \approx 3\xi$. As we shall see in the next section, a fitting form will prove useful when characterizing

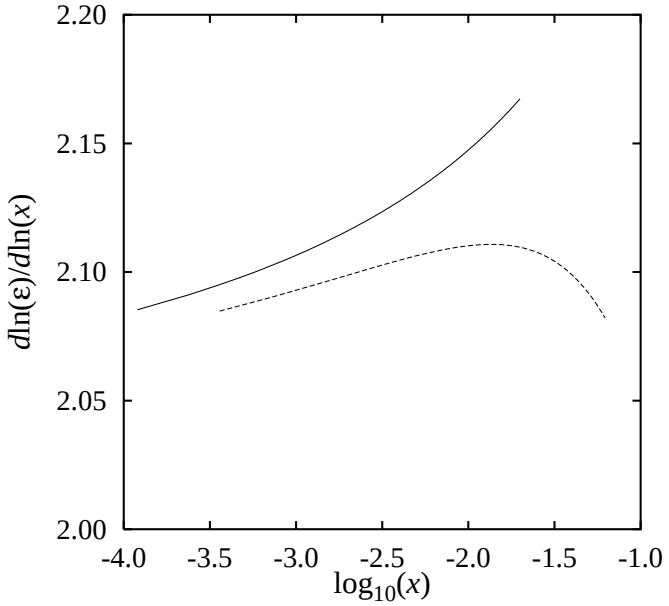

FIG. 7. The effective exponent characterizing the increase of the relative excess surface energy $d\ln\varepsilon/d\ln x$, where x is either the displacement ξ (solid), or a function of it $[1/(1-\xi)^3-1]$ (dashed). In both cases, the maximum value of ξ is 2%.

the behavior of the droplet for different configurations of compressing planes.

As can be seen by comparing the curves of Fig. 6 at low compressions, a power law describes the data very well, down to machine precision values at $\varepsilon \approx 10^{-8}$. The fitting curve (dotted) has an exponent $\alpha = 2.1$ and is obtained from fitting the data over a range covering more than an order of magnitude. The exact solution is contrasted with the other estimates which show a harmonic behavior ($\alpha = 2$) at small ξ. At larger ξ, the power law overestimates the excess energy but this occurs at $\xi \approx 0.2$. Nevertheless, the range of ξ over which a power law describes the data very well is more than two decades.

To investigate the validity of a power-law functional form for ε at very small compressions, we simplify Eq. 31 by taking one derivative with respect to ξ and integrating $f(\xi)$ to obtain

$$\xi = -\frac{1}{2} f \ln(f/4). \tag{33}$$

This allows us to define an effective exponent for very small compression

$$\frac{d\ln\varepsilon}{d\ln\xi} = \frac{\xi f}{\varepsilon} = \frac{2\ln(f/4)}{\ln(f/4)+1/2}, \tag{34}$$

characterizing the increase of the excess energy. The exponent is obtained in terms of f which can be numerically converted to ξ using Eq. 32. Figure 7 shows the ξ dependence of the effective exponent for the two different fitting forms we propose here. For both cases, points on the curve are bounded by $\xi < 2\%$, since these results are derived from the lowest-order expansion of the energy. In contrast to what is suggested by Fig. 6, the exponent is not constant for very small compression, but slowly decreases, going to 2 only at $\xi \to 0$. This notwithstanding, a power law with a fixed exponent provides a good approximation for the droplet potential over the range of values of ξ typically encountered in compressed emulsions.

IV. NUMERICAL RESULTS

Except for special cases, as shown in the previous section, the excess surface energy of a deformed droplet can only be determined numerically. Given the Surface Evolver software written by Brakke [9], it is relatively easy to calculate the shape of a single droplet with minimum surface area (energy) under the constraint of fixed droplet volume and as a function of confinement. We have obtained results for various confining polyhedral cells, some of which are Wigner-Seitz cells associated with standard packing structures. The surprising result of this study is that for a considerable range of compressions, the energy is well described by a power law, *where the exponent depends on the number of faces of the confining cell.*

The starting state is a spherical droplet which is composed of either 3074 or 12290 vertices. Most of the results presented here are for the latter case. The initial droplet is confined inside a polyhedral cell having between four and twenty faces. In particular, we used a rhombic dodecahedron (face-centered cubic), a truncated octahedron (body-centered cubic) and a simple cube (simple cubic), all of which are space-filling polyhedra. In addition, we compressed the droplet within a tetrahedron, an octahedron, a pentagon dodecahedron, and an icosahedron. Simpler structures were used as well, namely compression between a pair of parallel plates to compare to the results obtained in Sec. III, and between two perpendicular pairs of parallel plates. Results for two parallel plates are shown as the open circles in Fig. 4. As expected, they are in agreement with the analytic calculations down to very low compression where the change in surface area is comparable to the numerical uncertainty in SE. In all cases, the compressions leave the center of mass unchanged so that a distance h from the center can be defined.

Figure 8 shows the calculated dependence of the relative excess energy (Eq. 24) per facet, ε/n, on ξ (Eq. 2) for different types of confinement cells. n represents the number of compressing planes which is equivalent to the coordination number for space-filling cells. Using a fitting function of the form

$$\varepsilon/n = C\left[\left(\frac{R}{h}\right)^3 - 1\right]^\alpha, \tag{35}$$

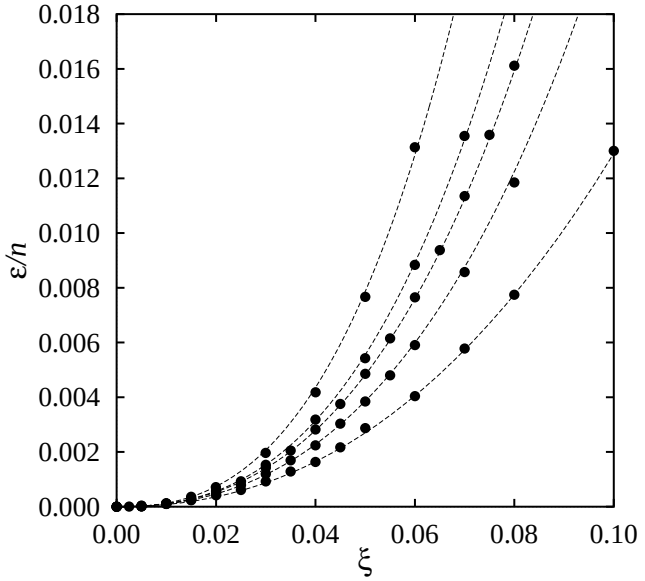

FIG. 8. Relative excess surface energy per facet, Eq. 24, for a single droplet as a function of the plate displacement, $\xi = (R - h)/R$. Curves are, from top to bottom, $n = 12$ (f.c.c.), 8 (low compression b.c.c.), 6 (s.c.), 4 (tetrahedron), 2 (2 plates). All curves are best fit to power law Eq. 35. Note that for clarity, not all cases of Table I are shown here.

we find that both the coefficient, C, and the exponent, α, depend on n, as indicated in Table I. As mentioned before, Eq. 35 is equivalent to $C'(\varphi - \varphi_c)^\alpha$ when the droplet is confined by space-filling polyhedra. As in the case of two parallel plates, this form fits the data better over a wider range than ξ^α. The data selected for the fit lie in the ξ interval 2–6%. This range was chosen to avoid errors associated with low values of ξ. On the other hand, the upper value fixes the range we are interested in. Indeed, since $\xi = 1 - (\varphi_c/\varphi)^{\frac{1}{3}}$, a face-centered-cubic structure (f.c.c., $\varphi_c = \pi\sqrt{2}/6$) for instance, has $\xi \approx 9.5\%$ in the dry foam limit $\varphi = 1$.

Our results explicitly show that the response of a droplet to compression is a non-local phenomenon: *the response depends on the number of planes used to compress the droplet*. In addition, one might expect it to depend on the relative positions of these planes, but it will be shown below that this effect is not very important. It is worth noting that since $\alpha(n) > 2$ for all cases, this response is weaker than a harmonic interaction: the response is equivalent to having the spring constant go to zero as the distortion vanishes. We also note that a power law with an exponent which increases as the number of compressing planes increases is unphysical for small compressions as the energy curves for different n would cross. Thus, although the fits shown in Fig. 8 appear convincing, the functional form should be viewed uniquely as a convenient way to mimic the response of a droplet.

In view of investigating the dependence of the relative positions of the compressing planes on the droplet, we obtained data for different configurations having the same

TABLE I. Values of the parameters C and α of the power-law fit to the relative excess energy (Eq. 35). The various configurations are ordered according to their coordination number n. Errors are in the last digit.

configuration	n	$C(10^{-3})$	α
pair of ∥ plates	2	7	2.1
two ⊥ pairs of ∥ plates	4	12	2.1
tetrahedron	4	14	2.1
cube (s.c.)	6	21	2.2
octahedron (low-φ b.c.c.)	8	27	2.3
rhombic dodecahedron (f.c.c.)	12	55	2.5
pentagonal dodecahedron	12	54	2.5
icosahedron	20	69	2.6

n. By comparing, say, the results of the f.c.c. structure to those of the pentagon dodecahedron, we see that the influence of the configuration on the fitting parameters is marginal compared to that of n. It therefore seems reasonable to conclude that, provided that the different facets of the droplet are not too close, the potential is only a function of the coordination number n. This information is valuable for modeling the excess energy of a droplet in a disordered emulsion [14]. A second point of interest is the saturation of the exponent α above $n \approx 12$. Although the number of neighbors nearly doubles from a rhombic dodecahedron to an icosahedron, the exponent barely changes.

In a similar way, by comparing the excess energy obtained by compressing a droplet in an octahedron to that obtained for the truncated octahedron, one can determine the importance of the second neighbors in the base-centered-cubic (b.c.c.) lattice. We find that second neighbors do not play a role for $\varphi \lesssim 0.90$ ($\xi \approx 6.3\%$). For $\varphi = 0.93$, the excess energy differences between the two is about 5%. Thus over most of the range of interest, only the eight nearest neighbors are relevant.

V. OPTIMAL PACKINGS FOR FOAM

Our numerical results also allow us to compare the energy of the various packings as a function of volume fraction. For a wide range of volume fractions, the lowest energy state of monodisperse emulsions is believed to be a packing of droplets in an f.c.c. structure. We neglect temperature effects in the following argument. For $\varphi > \varphi_m \approx 0.545$, i.e. the melting concentration of monodisperse hard spheres [22], up to $\varphi < \varphi_c = \pi\sqrt{2}/6 \simeq 0.7405$, i.e. close packing concentration, the droplets remain spherical in an f.c.c. structure as they can pack without touching. For $\varphi > \varphi_c$, the lowest energy state remains f.c.c. until it changes to a new structure at $\varphi^* < 1$. That such a crossover must exist is clear from previous work on dry foams.

In the limit $\varphi \approx 1$, an emulsion becomes a biliquid foam which is structurally analogous to a dry foam. The

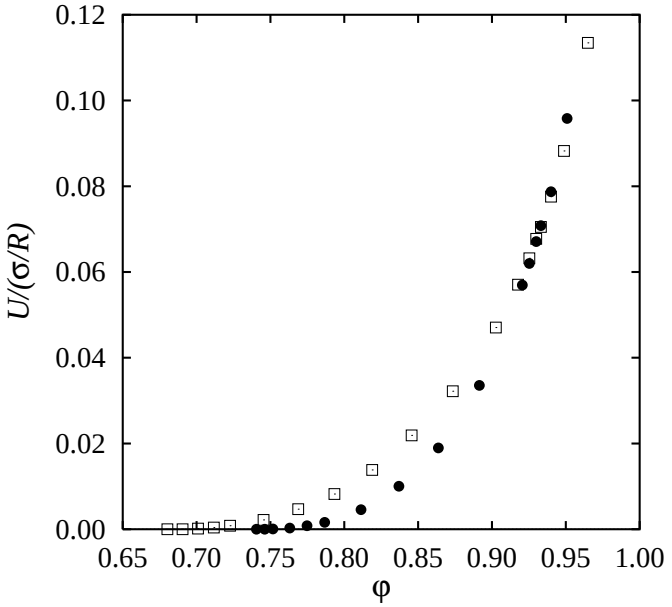

FIG. 9. The scaled excess energy density versus the volume fraction as extracted from a droplet in a b.c.c. (□) and f.c.c. (•) lattice. We find a crossover from f.c.c. to b.c.c. at $\varphi^* = 0.932(1)$. $\varphi_c = \pi\sqrt{3}/8 \simeq 0.6802$ for b.c.c. and $\pi\sqrt{2}/6 \simeq 0.7405$ for f.c.c.

lowest-energy state of the latter has long been the object of study. For nearly one hundred years, it was thought that the Kelvin [23] structure based on a b.c.c. packing of identical orthic tetrakaidecadedra gave an optimal space filling of cells of the same volume. The mechanical equilibrium requirements of the foam structure are contained in Plateau's rules [10]. To satisfy these rules, Kelvin showed that the faces of each cell are slightly distorted [23]: the six quadrilateral surfaces remain planar but curve their edges while the eight hexagonal surfaces, in addition to sharing the same curved edges, become non-planar surfaces of zero mean curvature. The reduction in surface area from the undistorted Wigner-Seitz cell is approximately 0.16% [24,25]. By using SE, Weaire and Phelan [26] recently showed the existence of a packing having an energy lower than the Kelvin structure. This space-filling packing consists of six 14-sided polyhedra and two 12-sided polyhedra, all of equal volume, packed in a simple cubic cell. This new structure, which is based on the cubic clathrate structure, has a surface energy approximately 0.3% less than that of Kelvin. For comparison, the f.c.c. structure has an energy 0.7% higher than the Kelvin structure [26].

Since we have studied only a single droplet in a Wigner-Seitz cell, we cannot address the stability of the Kelvin structure versus that of Weaire-Phelan for $\varphi < 1$. However, we can study the crossover from the f.c.c. packing to the b.c.c. Kelvin-like packing as φ increases. In Fig. 9, we plot the (scaled) energy density, U, defined by

$$U = E/V = 3\varphi\varepsilon(\sigma/R) \tag{36}$$

as a function of φ for a droplet in b.c.c. and f.c.c. structures. Here, E is the excess surface energy $E = \sigma(A - 4\pi R^2)$. As expected, the energy density of the f.c.c. structure is the lowest over a wide range of φ. But at $\varphi^* = 0.932(1)$, we observe a crossover to the b.c.c. structure. This result is in agreement with a similar prediction by Kraynik [27]. Note that this crossover value is obtained strictly from surface energy considerations and may be superseded by other stability criteria. Moreover, our calculation neglects some degrees of freedom since it strictly involves compressing a droplet inside a polyhedral cell. This is more restrictive than compressing many droplets caged by their neighbors, and thus we are in fact obtaining an upper bound on the energy. However, since the energy of a drop in the shape of a truncated octahedron is only 0.16% higher than the orthic tetrakaidecadedra of the Kelvin structure in the dry foam limit, the corrections to the crossover value resulting from the surface curvature of the films between the droplets should be small. Note that the crossover point is just above the volume fraction where second neighbors begin to play a role in the energy of a compressed droplet in the b.c.c. phase. Thus, while the six second neighbors contribute to increasing the deformation of a droplet and thereby the surface area, the overall energy of the b.c.c. structure is still lower than that of the f.c.c. structure for $\varphi > 0.932$. As we shall see in the next section, second neighbors in the b.c.c. structure are required for stability under shear deformation.

The little difference in energy shown in Fig. 9 is not specific to b.c.c. and f.c.c. pairs. In fact, it is interesting to compare the energy per droplet obtained for the regular pentagon dodecahedron (r.p.d.) to those obtained for the b.c.c. and f.c.c. lattices. Since the r.p.d. is not a space-filling object, φ represents the ratio of droplet to cell volume for this case. If one compares the energy per droplet as a function of the volume ratio, one finds that the results for the r.p.d. are almost indistinguishable from that of a truncated octahedron, i.e. the b.c.c. unit cell. In particular, results for the r.p.d. are lower than that for f.c.c. at high φ. This suggests that it may be favorable for a compressed monodisperse emulsion to generate short-range icosahedral order such as it exists in metallic glasses. This implies that as an emulsion is compressed, it is likely to undergo a glass transition reminiscent of that occurring in metallic glasses. Indeed, it is found to be very difficult to obtain an ordered monodisperse emulsion experimentally, indicative of the deep energy minimum of an amorphous state.

VI. RESPONSE TO SHEAR

We now turn to the response of a compressed droplet to an impressed shear strain. Since we are considering a single droplet, the scope of our method is limited to ordered lattices. All the space-filling confinement cells

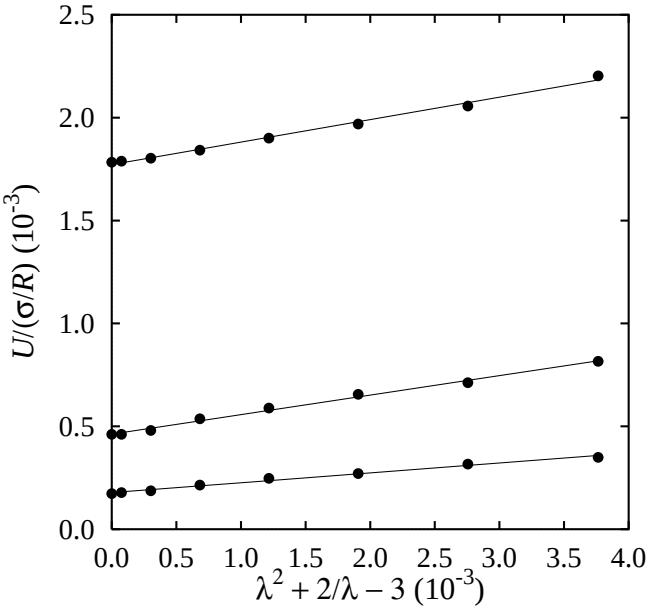

FIG. 10. Typical calculated excess energy density of a droplet compressed in an f.c.c. lattice as a function of shear strain. The strain is measured by $\lambda^2 + 2/\lambda - 3 \approx 3\epsilon^2$ so that the slopes are half the values of shear moduli [31]. Curves are for, top to bottom, $\varphi = 0.787$, 0.763, 0.746.

investigated here are related to the cubic point group and consequently, the associated elastic constant tensor is composed of three independent quantities. It is not possible for us to determine these constants individually.

A useful method for applying a shear strain in presence of periodic boundary conditions is to use an isochoric uniaxial compressional-extensional strain. The effective shear modulus can then be extracted from the resulting change in surface energy. The isochoric uniaxial strain consists in an extension of the Wigner-Seitz cell of $\lambda = 1 + \epsilon$ in the, say, z direction, associated with a compression of $\lambda^{-\frac{1}{2}}$ in the perpendicular plane. In principle, different orientations of the Wigner-Seitz cell with respect to the reference z axis would lead to effective measures of the modulus resulting from different combinations of the elastic constants. However, considerations of the alignment of the facets through periodic boundary conditions put restrictions on the possible orientations of the strains. Or, said differently, some orientations of the uniaxial strain involve forces that are not normal to the faces of the Wigner-Seitz cell, and it results that some facets do not lie on the cell boundary [5].

Here, the chosen orientation is along any of the three natural directions of a unit cell. For this particular choice, the strain tensor is written [28]

$$\gamma_{mn} = \frac{1}{2}\delta_{mn}(\lambda_m^2 - 1), \tag{37}$$

where δ_{mn} is the Kronecker delta, $\lambda_1 = \lambda_2 = \lambda^{-\frac{1}{2}}$, and $\lambda_3 = \lambda = 1 + \epsilon$. ϵ may be thought of as the magnitude of the small linear strain. The energy density U of the structure is given by

$$U = \frac{1}{2}\gamma_{mn}E_{mnpr}\gamma_{pr}, \tag{38}$$

where we use the summation convention. E is a fourth-order tensor which can be displayed as a 6×6 coefficient matrix using Voigt notation [5,29]. When a small isochoric uniaxial strain is applied, the energy density is found to vary as

$$U = \frac{3}{2}G\epsilon^2, \tag{39}$$

where the effective shear modulus G is the combination of the elastic constants $(C_{11} - C_{12})/2$. Our definition of G reduces consistently to the corresponding Lamé constant when considering an isotropic material.

Figure 10 shows a typical result for the variation of surface area as a function of shear strain for an f.c.c. lattice at different volume fractions. The strain is measured as $\lambda^2 + 2/\lambda - 3$ which is equivalent to $3\epsilon^2$ for small strains [31]. The slope of each curve is $G/2$.

In Fig. 11, the shear modulus is shown for the s.c. and f.c.c. lattices as a function of volume fraction. These results compare well with the ones obtained by Buzza and Cates [5] using Morse and Witten's potential [4]. Similar to what they found for a s.c. lattice, the shear modulus of the f.c.c. structure shows a smooth rise (rather than a jump) at φ_c. As we already mentioned, this behavior is different from that observed experimentally for disordered monodisperse emulsions.

The isochoric uniaxial strain is peculiar in that with $\lambda = 2^{\frac{1}{3}}$, it changes the metric tensor in such way to transform a b.c.c. lattice into an f.c.c. lattice with the same density [30]. The net energy required for this transformation will depend on the volume fraction as we have seen in the previous section when comparing the energy of both lattices. For $\varphi > \varphi_c$ and up to some $\varphi' < \varphi^*$, the b.c.c. structure was found to be unstable ($G < 0$) to an applied uniaxial strain. The existence of φ' derives from the stability of the b.c.c. lattice over the f.c.c. lattice for $\varphi > \varphi^*$. Second neighbors are responsible for stabilizing the structure against shear strain and it is not surprising to find that $\varphi' \gtrsim 0.90$, the point where second neighbors start touching the droplet. Our best estimate for φ', i.e. the volume fraction above which a b.c.c. lattice has a positive shear modulus for an isochoric uniaxial strain, is 0.903(5).

VII. DISCUSSION AND CONCLUSION

We have shown that the droplet response to small compressions in three dimensions is not harmonic and that it depends on the number of neighbors. For droplets compressed between two parallel plates, the surface profile can be solved analytically for small deformations and

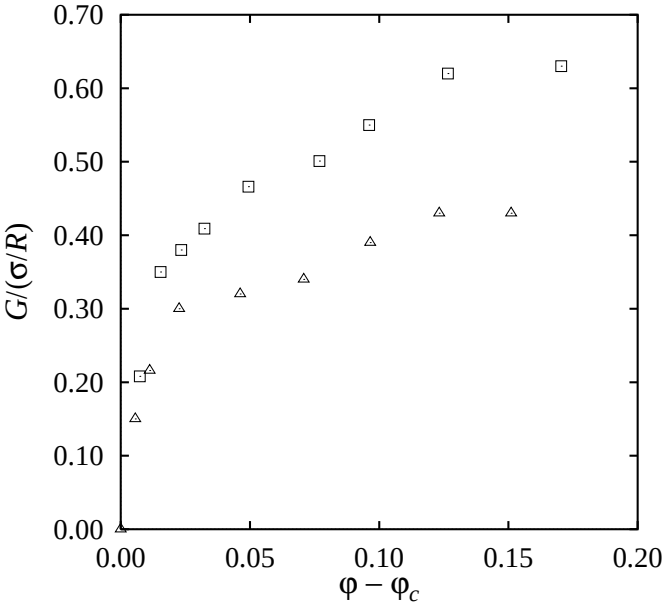

FIG. 11. Shear modulus for a droplet in s.c. (□) and f.c.c. (△) Wigner-Seitz confinement cells as a function of compression. Errors are of the order of 10%. $\varphi_c = \pi/6 \simeq 0.5236$ for s.c. and $\pi\sqrt{2}/6 \simeq 0.7405$ for f.c.c.

integrated numerically for arbitrary deformations. However for other geometries, the deformation can only be determined numerically. Using the Surface Evolver software [9], we have determined the change in surface area of droplets compressed in a variety of confining polyhedra. Our results strongly suggest that in three dimensions, though not in two, the response is non-local. The data fit very well with a non-harmonic scaling form in which the parameters of the fit depend almost exclusively on the coordination number. This feature has been used elsewhere [14] to build a pairwise inter-droplet potential in order to investigate the elastic response of disordered monodisperse emulsions.

The response to shear was also investigated for ordered lattices and it was found that similar to previous studies [5], the volume-fraction dependence of the shear modulus shows a rather sharp increase at the onset of droplet touching, φ_c. Although the anharmonicity of the potential certainly plays a role in the linear onset of G for disordered emulsions, it was shown here that it is not sufficient. The experimental results currently available [6,8] are for disordered emulsions only. Ordered lattices are easier to study theoretically but the effects of disorder seem to be too important to permit comparison with experiment. We have shown elsewhere [14] that both anharmonicity and disorder are required to reproduce the experimental results.

ACKNOWLEDGMENTS

We thank Shlomo Alexander, Wei Cheng Cai, Thomas Halsey, and David Weitz for useful discussions, and *Le Fonds FCAR du Québec* and the U.S.-Israel Binational Science Foundation for financial support.

[1] H.M. Princen, J. Colloid Interface Sci. **91**, 160 (1983).
[2] A.M. Kraynik, Ann. Rev. Fluid Mech. **20**, 325 (1988).
[3] F. Bolton and D. Weaire, Phys. Rev. Lett. **65**, 3449 (1990).
[4] D.C. Morse and T.A. Witten, Europhys. Lett. **22**, 549 (1993).
[5] D.M.A. Buzza and M.E. Cates, Langmuir **10**, 4503 (1994).
[6] T.G. Mason, J. Bibette, and D.A. Weitz, Phys. Rev. Lett. **75**, 2051 (1995).
[7] J.G. Berryman, Phys. Rev. A **27**, 1053 (1983) and references therein.
[8] H.M. Princen and A.D. Kiss, J. Colloid Interface Sci. **112**, 427 (1986).
[9] K. Brakke, Exp. Math. **1**, 141 (1992).
[10] J. Plateau, *Statique Expérimentale et Théorique des Liquides Soumis aux Seules Forces Moléculaires*, (Gauthier-Villars, Paris, 1873).
[11] S. Hutzler and D. Weaire, J. Phys.: Condens. Matter **7**, L657 (1995).
[12] D. Durian, Phys. Rev. Lett. **75**, 4780 (1995).
[13] H.M. Princen, M.P. Aronson, and J.C. Moser, J. Colloid Interface Sci. **75**, 246 (1980).
[14] M.-D. Lacasse, G.S. Grest, D. Levine, T.G. Mason, and D.A. Weitz, Phys. Rev. Lett. **76**, xxx (1996).
[15] D. Bideau and J.P. Troadec, J. Phys. C **17**, L731 (1984) and references therein.
[16] H.M. Princen, J. Colloid Interface Sci. **71**, 55 (1979).
[17] R.D. Gilette and D.C. Dyson, Chem. Engrg. J. **2**, 44 (1971).
[18] D.H. Michael, Ann. Rev. Fluid Mech. **13**, 189 (1981).
[19] T.I. Vogel, SIAM J. Appl. Math. **47**, 516, (1987); *Ibid.* **49**, 1009, (1989).
[20] L. Zhou, Ph.D. Dissertation, Stanford University (1995); preprints.
[21] R. Weinstock, *Calculus of variations* (Dover, New York, 1974).
[22] W.G. Hoover and F.H. Ree, J. Chem. Phys. **49**, 3609 (1968).
[23] W. Thomson (Lord Kelvin), Phil. Mag. **24**, 503 (1887).
[24] H.M. Princen and P.J. Levinson, J. Colloid Interface Sci. **120**, 172 (1987).
[25] D.S. Reinelt and A.M. Kraynik, J. Colloid Interface Sci. **159**, 460 (1993).
[26] D. Weaire and R. Phelan, Phil. Mag. Lett. **69**, 107 (1994).
[27] A.M. Kraynik, private communication.
[28] R.L. Bisplinghoff, J.W. Mar, and T.H.H. Pian, *Statics of deformable solids* (Dover, New-York, 1990).
[29] L. Landau and E. Lifshitz, *Theory of Elasticity* (Pergamon, Oxford, 1959).
[30] A. Rahman and G Jacucci, Nuovo Cimento D **4**, 357 (1984).
[31] L.R.G. Treloar, Rep. Prog. Phys. **36**, 755 (1973).